PROCEEDINGS, 43rd Workshop on Geothermal Reservoir Engineering
Stanford University, Stanford, California, February 12-14, 2018
SGP-TR-213

Numerical Simulation Applications in the Design of EGS Collab Experiment 1

Mark D. White[1], Pengcheng Fu[2], Ahmad Ghassemi[3], Hai Huang[4], Jonny Rutqvist[5], Bud Johnston[6], EGS Collab Team[7]

[1]Energy and Environment Directorate, Pacific Northwest National Laboratory, Richland, WA 99352, USA

[2]Atmospheric, Earth and Energy Division, Lawrence Livermore National Laboratory, Livermore, CA 94550, USA

[3]Petroleum and Geologic Engineering, The University of Oklahoma, Norman, OK 94550, USA

[4]Energy and Environment Science and Technology Directorate, Idaho National Laboratory, Idaho Falls, ID

[5]Earth and Environmental Sciences, Lawrence Berkeley National Laboratory, Berkeley, CA 94720, USA

[6]Geothermal Technologies Program, National Renewable Energy Laboratory, Golden, CO 80401, USA

Email: mark.white@pnnl.gov

Keywords: Numerical Simulation, EGS Collab, EGS, Sanford Underground Research Facility, Meso-Scale Experimental Design, Stimulation, Circulation, Hydraulic Fracture, Borehole Orientation, Borehole Notching, THMC Modeling

ABSTRACT

The United States Department of Energy, Geothermal Technologies Office (GTO) is funding a collaborative investigation of enhanced geothermal systems (EGS) processes at the meso-scale. This study, referred to as the EGS Collab project, is a unique opportunity for scientists and engineers to investigate the creation of fracture networks and circulation of fluids across those networks under in-situ stress conditions. The EGS Collab project is envisioned to comprise three experiments and the site for the first experiment is on the 4850 Level (4,850 feet below ground surface) in phyllite of the Precambrian Poorman formation, at the Sanford Underground Research Facility, located at the former Homestake Gold Mine, in Lead, South Dakota. Principal objectives of the project are to develop a number of intermediate-scale field sites and to conduct well-controlled in situ experiments focused on rock fracture behavior and permeability enhancement. Data generated during these experiments will be compared against predictions of a suite of computer codes specifically designed to solve problems involving coupled thermal, hydrological, geomechanical, and geochemical processes. Comparisons between experimental and numerical simulation results will provide code developers with direction for improvements and verification of process models, build confidence in the suite of available numerical tools, and ultimately identify critical future development needs for the geothermal modeling community. Moreover, conducting thorough comparisons of models, modelling approaches, measurement approaches and measured data, via the EGS Collab project, will serve to identify techniques that are most likely to succeed at the Frontier Observatory for Research in Geothermal Energy (FORGE), the GTO's flagship EGS research effort. As noted, outcomes from the EGS Collab project experiments will serve as benchmarks for computer code verification, but numerical simulation additionally plays an essential role in designing these meso-scale experiments.

This paper describes specific numerical simulations supporting the design of Experiment 1, a field test involving hydraulic stimulation of two fractures from notched sections of the injection borehole and fluid circulation between sub-horizontal injection and production boreholes in each fracture individually and collectively, including the circulation of chilled water. Whereas the mine drift allows for accurate and close placement of monitoring instrumentation to the developed fractures, active ventilation in the drift cooled the rock mass within the experimental volume. Numerical simulations were executed to predict seismic events and magnitudes during stimulation, initial fracture orientations for smooth horizontal wellbores, pressure requirements for fracture initiation from notched wellbores, fracture propagation during stimulation between the injection and production boreholes, tracer travel times between the injection and production boreholes, produced fluid temperatures with chilled water injections, pressure limits on fluid circulation to avoid fracture growth, temperature environment surrounding the 4850 Level drift, and fracture propagation within a stress field altered by drift excavation, ventilation cooling, and dewatering.

1. INTRODUCTION

In October 2016, the United States Department of Energy (DOE), Geothermal Technologies Office (GTO) announced a funding opportunity that was to be collaborative in nature and act as a research and development path between laboratory-scale stimulation and

[7] J. Ajo-Franklin, S.J. Bauer, T. Baumgartner, K. Beckers, D. Blankenship, A. Bonneville, L. Boyd, S.T. Brown, J.A. Burghardt, T. Chen, Y. Chen, K. Condon, P.J. Cook, P.F. Dobson, T. Doe, C.A. Doughty, D. Elsworth, J. Feldman, A. Foris, L.P. Frash, Z. Frone, P. Fu, K. Gao, A. Ghassemi, H. Gudmundsdottir, Y. Guglielmi, G. Guthrie, B. Haimson, A. Hawkins, J. Heise, C.G. Herrick, M. Horn, R.N. Horne, J. Horner, M. Hu, H. Huang, L. Huang, K. Im, M. Ingraham, T.C. Johnson, B. Johnston, S. Karra, K. Kim, D.K. King, T. Kneafsey, H. Knox, J. Knox, D. Kumar, K. Kutun, M. Lee, K. Li, R. Lopez, M. Maceira, N. Makedonska, C. Marone, E. Mattson, M.W. McClure, J. McLennan, T. McLing, R.J. Mellors, E. Metcalfe, J. Miskimins, J.P. Morris, S. Nakagawa, G. Neupane, G. Newman, A. Nieto, C.M. Oldenburg, W. Pan, R. Pawar, P. Petrov, B. Pietzyk, R. Podgorney, Y. Polsky, S. Porse, S. Richard, M. Robertson, W. Roggenthen, J. Rutqvist, D. Rynders, H. Santos-Villalobos, P. Schwering, V. Sesetty, A. Singh, M.M. Smith, H. Sone, C.E. Strickland, J. Su, C. Ulrich, N. Uzunlar, A. Vachaparampil, C.A. Valladao, W. Vandermeer, G. Vandine, D. Vardiman, V.R. Vermeul, J.L. Wagoner, H.F. Wang, J. Weers, J. White, M.D. White, P. Winterfeld, T. Wood, H. Wu, Y.S. Wu, Y. Wu, Y. Zhang, Y.Q. Zhang, J. Zhou, Q. Zhou, M.D. Zoback

rock mechanics studies and the large field scale of the future Frontier Observatory for Research in Geothermal Energy (FORGE) investigations (U.S. Department of Energy, 2017). The recipient of the Collab award was announced in early 2017, the Stimulation Investigations for Geothermal Modeling Analysis and Validation (EGS COLLAB) project, led by the Lawrence Berkeley National Laboratory (LBNL). This collaborative project involves national laboratories, universities and private industry teaming to conduct stimulation and circulation experiments, and verify computer codes, numerical algorithms and approaches, and process models against the generated data. This three-year project has been tasked with providing new knowledge and modeling capabilities, forming a path from laboratory scale to the field scale of FORGE.

Code verification is a critical element in the advancement of numerical simulators for enhanced geothermal systems (EGSs). DOE has supported the development and verification of numerical simulators throughout the history of EGS research, starting with the Finite Element Heat and Mass (FEHM), HDR Heat, and GEOCRACK models (Duchane and Winchester, 1993; Zyvoloski, 2007), used to estimate the potential thermal lifetime of the Phase II Reservoir at Fenton Hill. More recently GTO sponsored a multiple-year code comparison study that considered seven benchmark problems and two challenge problems (White et al., 2017a; White et al., 2016). The benchmark problems were structured to test the ability of the collection of numerical simulators to solve various combinations of coupled thermal, hydrologic, geomechanical, and geochemical processes. This class of problems was strictly defined in terms of properties, driving forces, initial conditions, and boundary conditions.

The two challenge problems were based on the Fenton Hill Hot Dry Rock (HDR) (Brown et al., 2012) project, where the stimulation, completion, and circulation testing in two separate reservoirs, distinguished by depth and flow complexity, were conducted. Both challenge problems have specific questions to be answered via numerical simulation in three topical areas: 1) reservoir creation/stimulation, 2) reactive and passive transport, and 3) thermal recovery. Whereas the benchmark class of problems were designed to test capabilities for modeling coupled processes under strictly specified conditions, the stated objective for the challenge class of problems was to demonstrate what new understanding of the Fenton Hill experiments could be realized via the application of modern numerical simulation tools by recognized expert practitioners. Critical observations and data from the Fenton Hill experiments were varied and scattered among a number of individual experiments, and numerical simulation solutions were sought that satisfied as many observations at possible. Achieving agreement in multiple experimental observations from Fenton Hill often required participants to critically think about stimulation mechanisms involving natural and hydraulic fractures and re-evaluate their conceptual models and numerical solution approaches. This process has yielded new insights to Fenton Hill reservoirs and direction for future EGS research.

The EGS Collab project is a recognition of the importance of validating numerical simulation tools for EGS, and the meso-scale of the experiments and accessibility of the generated fracture networks under in-situ stress conditions and crystalline rock formations provides a unique opportunity for the validation of THMC modeling approaches. The EGS Collab project comprises three major experiments, occurring over the course of the three-year project duration. Each major experiment is composed of a series of smaller stimulation and circulation experiments. Prior to each experiment site characterization will be conducted and numerical simulations will be executed to guide the experimental design and monitoring systems. After each experiment, numerical simulations will be executed and results compared against the collected data. The diversity of the EGS Collab teams brings a spectrum of numerical approaches for modeling THMC processes for EGS (White et al., 2016). The post experimental period will allow for comparison of these numerical approaches and an assessment of code limitations, need for code improvements, or alterations to conceptual models.

EGS Collab Experiment 1 is being conducted with a volume of predominately phyllite rock on the western side of the 4850 Level (4,850 feet below ground surface) West Access Drift (drift) within Sanford Underground Research Facility (SURF) near the kISMET site (Oldenburg et al., 2016). This experiment involves two stages: 1) stimulation - the creation of a hydraulic fracture sub-horizontal borehole drilled nominally in the direction of the principal minimum compressive horizontal stress (i.e., σ_h); and 2) circulation – the circulation of fluids between an injection well and one or more production wells intersecting the created fracture. At this writing, a series of eight boreholes have been drilled from the drift: 1) injection [E1-I], 2) production [E1-P], 3) two fracture orthogonal monitoring [E1-OT, E1-OB], 4) two deep fracture parallel monitoring [E1-PDT, E1-PDB], and 5) two shallow fracture parallel monitoring [E1-PST, E1-PSB]. The injection and production boreholes were drilled in the anticipated direction of σ_h, (i.e., with a 356° trend and 12° plunge). The two fracture orthogonal monitoring wells were drilled with the same azimuth of σ_h, (i.e., with a 356° trend), but at higher and lower plunges, forming a vertical "v" shape with the apex at the drift wall. Each pair of fracture parallel monitoring wells were drilled orthogonal to the injection and production boreholes, forming a 12° tilted "v" shape with the apex at the drift wall. Numerical simulations have played informative role in designing this first hydraulic stimulation and circulation experiment, being called upon to answer specific questions:

1. What is the preferred orientation for the stimulation borehole to meet the project objectives?
2. What anticipated number and magnitudes of seismic events during hydraulic stimulation?
3. What flow rates and pressures should the circulation experiments be executed to prevent fracture propagation?
4. What circulation duration is required to achieve measureable temperature changes in the production borehole?
5. Can the production well serve to prevent fracture propagation to the drift?
6. Will a transverse hydraulic fracture form from the unaltered injection borehole drilled in the direction of σ_h, or is notching required?
7. How does notch geometry impact stimulation pressure and near wellbore impedance?
8. What is the thermal profile around the drift?
9. How is the stress state altered in the experimental volume via mechanical and thermal alteration from the mine workings and drift cooling?
10. What is the anticipated shape and arrival time in terms of injected fluid volume of the hydraulically generated fracture under the mechanically and thermally altered stress state?

Six teams executed numerical simulations to address these questions: 1) Idaho National Laboratory (INL), 2) Lawrence Berkeley National Laboratory (LBNL), 3) Lawrence Livermore National Laboratory (LLNL), 4) National Renewable Energy Laboratory (NREL) and Colorado School of Mines (CSM), 5) Pacific Northwest National Laboratory (PNNL), and 6) University of Oklahoma (OU). Numerical simulations addressing the first five questions listed above were previously published (White et al., 2017b), and the outcomes are summarized below. This paper describes numerical simulations executed by multiple teams to provide quantitative and informative answers to the last five questions listed above, with the two notch questions grouped under one section.

1.1 Borehole Orientation

Current estimates of the *in-situ* stress state at the first experiment site on the 4850 Level at SURF are σ_v = 41.8 MPa (Oldenburg et al, 2016), σ_h = 21.7 MPa, with a 356° trend and 12° plunge indicating fractures that are striking N86°E with a dip of 78° to the southeast (Oldenburg et al, 2016), and σ_H = 33.4 – 37.6 MPa. The kISMET stimulation borehole was drilled nearly vertical and the near vertical fracture that resulted from hydraulic stimulation had a surface normal generally oriented toward the direction of σ_h, with little influence in orientation on rock fabric. In applying their GeoFrac 2D and 3D models, the OU team determined that for stimulation boreholes drilled in the direction of σ_h it would not be possible to initiate a transverse fracture, indicating notching is needed. Likewise the team from INL in applying their finite-element geomechanics capabilities of the FALCON (Fracturing And Liquid CONvection) (Gaston et al. 2012a,b; Podgorney et al. 2010) code determined for a horizontal or sub-horizontal borehole oriented in the direction of σ_h, and σ_H close in value to σ_v that notching the borehole would reduce the fracture initiation pressure and yield a fracture preferentially oriented in the transverse direction to the borehole.

1.2 Seismic Events and Magnitudes

A requirement for conducting work underground at SURF is an approved experimental plan and an element of that plan is an estimation of potential micro-seismicity resulting from the hydrofracture experiments. The question of what the anticipated number and magnitude of seismic events associated with the hydraulic stimulation was answered with numerical simulations executed with a fully coupled three-dimensional network flow and quasi-static discrete element model (DEM) (Zhou et al., 2017). The simulation is initialized by imposing the *in-situ* stresses as strain energy in the elastic beams connecting the DEM particles. As the beams break with fluid injection, this strain energy is released. Estimates of the magnitude of the seismic events that occurred during the stimulation were developed by considering each beam break as an event, or by summing the released energy over a time step. The outcome from these simulations forecasted a maximum energy release during stimulation to occur during the initial fracture opening state of about 37.5 kJ, which is equivalent to a 0.1 magnitude on the Richter scale. The simulations additionally showed that after the initial opening, the fracture propagates smoothly (on average) under constant rate injection, with a few relatively large events.

1.3 Circulation Experiments without Fracture Growth

To design the circulation experiments, particularly to make equipment procurement plans and calculate circulation durations, it is necessary to have an estimate of the expected circulation rate. It is desired to have a relatively high circulation rate to be able to observe thermal breakthrough within a reasonable experiment time. A constraint is that injection pressure during circulation tests should not be high enough to propagate the fracture. The LLNL team estimated achievable circulation rates for two scenarios: 1) assuming homogeneous in situ stress distribution and an idealized penny-shaped fracture, and 2) assuming a heterogeneous stress field and a somewhat irregular fracture shape. Using its GEOS code (Settgast et al. 2017; Fu et al., 2013), the LLNL team demonstrated that the highest flow that could be achieved across the fracture without incurring continued fracture propagation was achieved when the back-pressure is slightly lower than σ_h for the homogeneous stress field. For the heterogeneous stress field, the simulations show that the maximum achievable circulation rate without continuing to propagate the fracture is likely below 0.01 L/s. When spatial variation of stress is significant, there exists the risk of production wellbore encountering the fracture at a high stress region and the circulation rate might be one order of magnitude lower than the maximum value.

1.4 Circulation Duration for Thermal Breakthrough and Conservative Tracer Response

Circulation duration for thermal breakthrough was modeled by LLNL and NREL/CSM teams. Low, moderate and high circulation rates were modeled using an idealized penny-shaped fracture with constant aperture. At low anticipated rates below 0.01 L/s, these idealized models indicate months or years are required to achieve a 1°C drop in produced fluid temperature. Thermal breakthrough is delayed due to a conduction-dominated mode of thermal decline at rates below 0.01 L/s. In addition to thermal breakthrough, the NREL/CSM team modeled conservative tracer response at multiple circulation rates below 0.01 L/s, and these idealized models indicate produced tracer concentrations peak within 2 hours following the start of slug injection. In summary, at rates below 0.01 L/s idealized models predict rapid conservative tracer response; however, a conduction-dominated mode of thermal decline severely delays thermal breakthrough.

1.5 Production Well Impacts on Fracture Propagation

The EGS Collab Experiment 1 site provides excellent access to the experimental volume of rock via the 4850 Level drift. The drift is sufficiently wide at the experimental site to permit horizontal and sub-horizontal drilling of monitoring boreholes at a variety of azimuths and dips. The experiment is designed to yield a near planar fracture orthogonal to the direction of σ_h which is only 37.5˚ off the direction of the 4850 Level West Access drift axis. At the design stimulation depth of 60 m, the fracture would initiate approximately 50 m from the drift wall. A component of the experimental design was to position and utilize the production borehole as a barrier for fracture migration to the drift wall. The LLNL team, with its GEOS code, investigated the ability of the production borehole to arrest fracture propagation toward the drift. The experimental protocol strategy was to maintain the production borehole at a constant pressure, slightly below σ_h, via a combination of a low-flow injection pump and a pressure relief valve, and then monitoring for fracture arrival at the production borehole via a change in drainage flow rate out the pressure relief valve. Numerical simulations were executed to address three questions: 1) what impact does production borehole drainage have on continued fracture propagation, 2) what is the drainage rate from

the production borehole at fracture arrival, and 3) what are the effects of back-pressure and injection rate? Conclusions from the simulations indicated the production borehole could serve as a barrier to continued fracture propagation:

1. By acting as a drain, a pressure-controlled production well is expected to be effective in halting fracture growth beyond the intersection.
2. The flow rate into the drainage well is not very sensitive to the back-pressure applied in the well.
3. The halting effects of the drainage well are more significant for lower injection rate.
4. For very low injection rate (e.g., 0.02 L/s), the drainage rate can be 70% of the injection rate and fracture growth in other directions are also substantially impeded.
5. If a five-spotted configuration is adopted, the overall fracture growth can be halted in almost all directions.

2. BOREHOLE NOTCHING

After the EGS COLLAB team reached a consensus that a horizontal (or sub-horizontal) borehole along the σh direction would provide a desired relative orientation between the wells and the fracture, thereby reducing near-well pressure loss during circulation, the LLNL modeling team worked closely with the Sandia drilling experiment team to investigate the optimization of wellbore notching design that generates stress concentration. Such stress concentration is necessary for initiating a hydraulic fracture perpendicular to the wellbore direction because pressurization of a smooth wellbore, cylindrical in shape, has very little effects on the axial stress along the wellbore, according to Kirsch's equations. Various notching mechanisms had been considered, including abrasive perforation, shape charges, and mechanical notching. Due to the desire to avoid explosives and logistic complexities, mechanical notching is being considered as a favorable solution. The objective of the study documented in the current section is to quantify the effects of notch geometries on stress concentration near the notch when both the wellbore and the notch are subjected to fluid pressure.

Per discussion with designers of the perspective notching device at Sandia National Laboratories, we consider the geometry shown in Figure 1(a) is considered. We first assume a smooth semi-circular cross-section. Although the actual notch is likely to have sharp, irregular shapes, we analyze the smooth shape for the following considerations:

1. The smooth shape induces stress concentration but not stress singularity, allowing robust stress analysis less sensitive to mesh resolution and also permits direct comparison between different geometries.
2. The smooth shape represents the "worst-case scenario". If tensile stress can be generated by this shape, the stress caused by a rough surface with the same depth (H) and width (W) is likely to be more favorable for fracture initiation.
3. What the results reveal is essentially for a given notch front geometry (smooth or shape), how the notch depth and width affect the stress concentration.

In addition to the stress analysis, we perform a parallel fracture mechanics analysis by introducing a small fracture, 4 mm deep, around the notch as shown in Figure 1(b). The stress analysis and fracture mechanics analysis results should be interpreted in a unified, mutually complementary fashion. Having sufficient tensile stress (in comparison with tensile strength of the rock) at the crown of the notch would result in a small fracture like that depicted in Figure 1(b), but this is not a sufficient condition for continued fracture growth as the generation of the small fracture could relax the stress concentration. Therefore, the role of the fracture mechanics analysis is to see if sufficient stress singularity (quantified by stress intensity factor in comparison with toughness of the rock) can be generated at the tip of the small fracture.

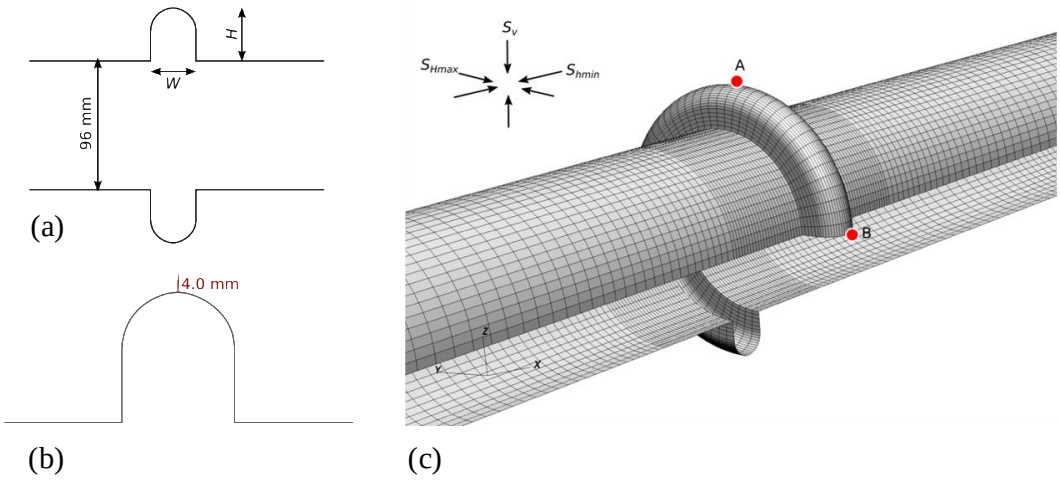

Figure 1: Notch geometry considered in this analysis. (a) A smooth notch surface for stress analysis with notch depth *H* and notch width *W* as variables. (b) Assuming a 4-mm deep crack at the crown of the smooth notch for fracture mechanics analysis. Illustration not to scale, (c) Mesh of the "skin" of the wellbore and notch with H = 20 mm and W = 20 mm.

We assume the rock to be linearly elastic and isotropic. The packed-off wellbore is 0.8 m long and 96 mm in diameter. The simulation domain is a cylinder 4.8 m long and 4.0 m in diameter, sufficiently large (to represent the far field rock) compared with the wellbore

geometry. Fluid pressure is applied on the surface of the wellbore, the two ends of the packed-off interval, the surface of the notch, and both walls of the 4-mm crack if applicable. The mesh of the "skin" of the wellbore and the notch is shown in Figure 1(c). We establish a coordinate system with the x-axis along the σ_h direction, y-axis along σ_H and z-axis pointing upwards. The symmetry in the system dictates that the highest tensile stress should emerge at either point A (top) or point B (side). The mesh resolution near the notch is 1 to 2 mm and larger elements are used in the far-field. The whole model includes approximately 1.6 million elements. Material properties are based on the kISMET report with Young's modulus of 71.4 GPa and Poisson's ratio of 0.22.

Taking advantage of the linearity of the system, instead of analyzing the stress state under a specific set of assumed *in situ* stress and fluid pressure, we derive, through finite element analysis, the "transfer function" from individual stress/pressure components to the response of interest, e.g. σ_x^A or tensile stress at point A in the x-direction, namely

$$\sigma_x^A = T_h\sigma_h + T_H\sigma_H + T_V\sigma_V + T_P P \quad (1)$$

where T_h, T_H, T_V, and T_P are the four coefficients of the transfer function. Note that each coefficient is a function of the notch geometry. Once we obtain the values of these coefficients, we can calculate the stress of interest for any combination of in situ stress and wellbore pressure. First, we consider the tensile stress at point A (σ_x^A). We simulate nine geometries as summarized in Table 1 and obtain the transfer function coefficients. Note that due to symmetry, the coefficients for point B are identical to those for A except that T_H and T_V are swapped.

Table 1 Coefficients for the transfer function for tensile stress at point A. The last column shows the tensile stress value corresponding to σ_h = 21.7 MPa, σ_H = 35.5 MPa, σ_V = 41.8 MPa, and P = 35 MPa.

H (mm)	W (mm)	T_h	T_H	T_V	T_P	$\boldsymbol{\sigma_x^A}$ (MPa)
20	20	-2.842	-0.355	0.683	1.513	7.22
30	20	-3.212	-0.266	0.659	1.818	12.04
40	20	-3.511	-0.199	0.638	2.071	15.90
50	20	-3.767	-0.150	0.622	2.293	19.19
60	20	-3.995	-0.116	0.611	2.496	22.06
20	30	-2.554	-0.293	0.634	1.212	3.10
60	30	-3.531	-0.078	0.596	2.000	15.52
20	10	-3.348	-0.500	0.776	2.071	14.50
60	10	-4.808	-0.406	0.620	3.402	32.97

As an example, when σ_h = 21.7 MPa, σ_H = 35.5 MPa, σ_V = 41.8 MPa, and wellbore pressure P = 35 MPa, for notch geometry of H = 20 mm and W = 20 mm, the tensile stress at point A is

$$\sigma_x^A = (-2.842)(21.7) + (-0.355)(35.5) + (0.683)(41.8) + (1.513)(35.0) = 7.22 \text{ MPa} \quad (2)$$

and at B is

$$\sigma_x^B = (-2.842)(21.7) + (0.683)(35.5) + (-0.355)(41.8) + (1.513)(35.0) = 0.68 \text{ MPa} \quad (3)$$

The calculated stress values for other notch geometries under the same stress/pressure condition are summarized in the last column on Table 1. For all geometries assumed, the applied wellbore pressure 35 MPa is able to generate significant tensile stress around the notch. Deeper and narrower notch geometries tend to generate greater tensile stress. The results of an actual finite element simulation directly using these parameters are shown in Figure 2(a). If we reduce the wellbore pressure to 27 MPa, three of the nine configurations will generate a tensile stress, where the other six configurations result in compression around the notch (results not shown but can be calculated quickly using the coefficients in Table 1). Results for the fracture mechanics analysis are summarized in Table 2. Note that the T_x values in Table 2 are dimensionless, whereas the K_x values in Table 2 has a unit of $m^{0.5}$.

A concern of the EGS COLLAB team was that whether an axial fracture would develop and propagate before a transverse fracture can be initiated from the notch. The fluid pressure chosen for this analysis, namely 35 MPa, is lower than both σ_H and σ_V, which guarantees that no axial fracture can propagate under this pressure. As this pressure, can generate sufficient tensile stress for all the notch geometries examined, it proves that a transverse fracture will be generated from the notch before an axial fracture propagates from the wellbore. This conclusion applies even if there already exists an axial fracture or a fracture that intersects the wellbore and is sub-parallel to the wellbore.

Table 2. Coefficients for the transfer function of stress intensity factor near point A. The last column shows the stress intensity factor value corresponding to σ_h = 21.7 MPa, σ_H = 35.5 MPa, σ_V = 41.8 MPa, and P = 35 MPa.

H (mm)	W (mm)	K_h	K_H	K_V	K_P	SIF^A(MPa)
20	20	-0.2384	-0.0307	0.0527	0.2156	3.49
30	20	-0.2688	-0.0235	0.0496	0.2419	3.87
40	20	-0.2935	-0.0181	0.0469	0.2638	4.18
50	20	-0.3148	-0.0139	0.0448	0.2831	4.46
60	20	-0.3338	-0.0107	0.0431	0.3066	4.70
20	30	-0.2292	-0.0265	0.0527	0.2022	3.36
60	30	-0.3168	-0.0067	0.0469	0.2759	4.51
20	10	-0.2461	-0.0378	0.0519	0.2310	3.57
60	10	-0.3490	-0.0172	0.0365	0.3289	4.85

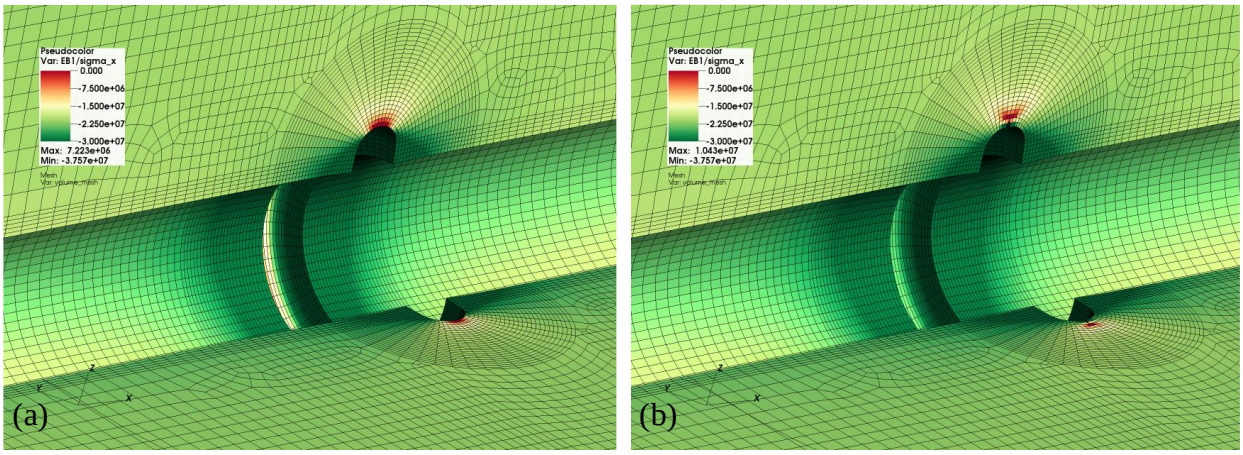

Figure 2: σ_x in the rock around the wellbore and the notch assuming σ_h = 21 MPa, σ_H = 40 MPa, σ_V = 42 MPa, and wellbore pressure P = 35 MPa for (a) smooth notch surface and (b) notch with a 4-mm deep crack around the notch. Deformation is magnified by 300 times.

3. THERMAL ENVIRONMENT SURROUNDING THE DRIFT

The volume of phyllite selected for Experiment 1 of the EGS Collab project is adjacent to the 4850 West Access Drift (drift). Ambient temperatures at the 4850 Level, determined from the Homestake mine surveys, are approximately 34˚C. Drifting activities started at the 4850 Level in 1949 and a variety of active cooling systems were used to reduce working temperatures for the miners. Gold mining operations ceased in Homestake mine in 2001 and the dewatering pumps were switched off in 2003. In 2007 the National Science Foundation approved the Deep Underground Science and Engineering Laboratory (DUSEL), which sought to establish an interim research facility at the 4850 Level and ultimately a deeper facility at the 8000 Level. With the establishment of DUSEL and then later the Sanford Underground Research Facility (SURF) dewatering pumps were switched on, and the water level in the mine reached the 4850 Level on May 13, 2009 (Dobson and Salve, 2009). Ventilation supplied from the Yates and Ross shafts serve to cool the open mine workings. The temperature profiles surrounding the 4850 Level drift are a function of the early mining activities from 1949 through 2003, the mine closure from 2003 to 2009, and then the reopening of the 4850 Level for scientific and engineering research from 2009 to present. Predictions of the temperature profile around the 4850 Level drift were made via numerical simulation for use in modeling fracture stimulation and thermal circulation experiments. Temperature measurements taken during the underground reconnaissance for the DUSEL facility (Dobson and Salve, 2009) and during the EGS-Collab project within the kISMET boreholes (Oldenburg et al., 2016; Roggenthen and King, 2017) were used for verification of the numerical simulation results. Teams from INL, LBNL, and PNNL developed solutions for temperature profiles around the 4850 Level.

3.1 INL Modeling and Simulation Team Study

The INL team developed 3-dimensional computational domain of 2.5 million tetrahedral elements, using Cubit (Blacker et al., 2017), that comprised the drift triangle on the 4850 Level between the Yates and Ross shafts, a volume of 2000 m x 1800 m x 600 m. Simulations were then executed with the FALCON code (Xia et al., 2017) as part of a combined thermo-mechanical analysis to model stress alterations due to the presence of drifts and thermal cooling. The lateral boundaries of the computational domain were fixed at the geothermal gradient

of the Homestake mine survey and the air temperature in the drift was fixed at 20.11˚C. Simulations were executed for a period of 50 years, with constant parameters, listed in Table 3. Simulation results showed good agreement against the kISMET survey (Roggenthen and King, 2017), as shown in Figure 3.

Table 3. INL Simulation Parameters

Parameter	Value	Parameter	Value
Rock Specific Heat	775 J/kg K	Rock Density	2730 kg/m^3
Heat Transfer Coefficient	5 W/m^2 K	Rock Thermal Conductivity	4.5 W/m K

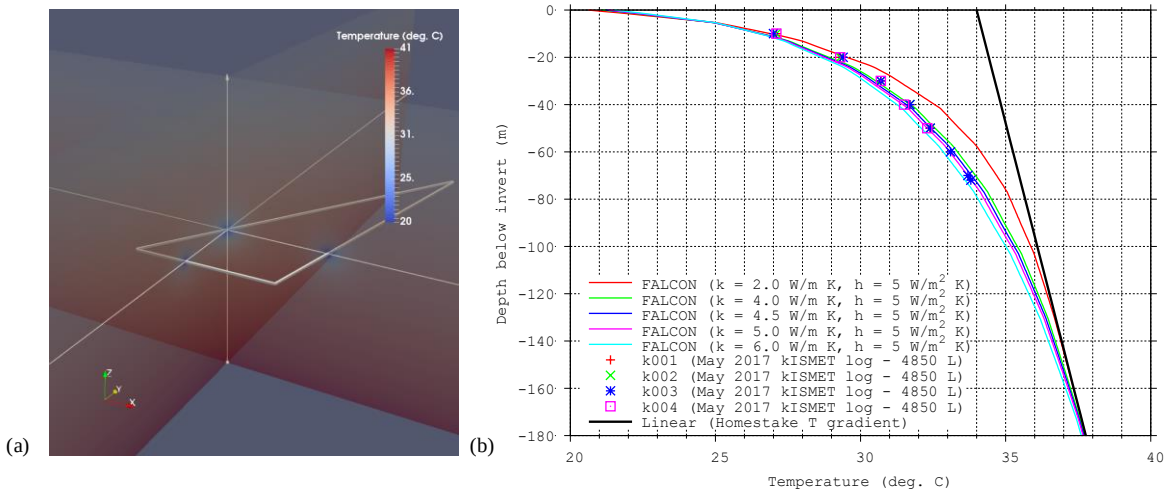

Figure 3: INL thermal simulation results, (a) 3-dimensional domain at 50 years with kISMET well shown as line A-B, (b) comparison with kISMET well survey.

3.2 LBNL Modeling and Simulation Team Study

The LBNL team developed a 3-dimensional computational domain with a volume of 500 m x 500 m x 500 m, aligned with the 4850 Drift, but oblique to the current estimate of the principal stress field. Simulations were executed with the TOUGH-FLAC simulator (Rutqvist, 2011), as a combined thermo-hydro-mechanical modeling study to quantify the impact of the drift, in terms of stress redistribution due to the drift excavation itself, as well as due to cooling and drainage (pressure) induced stress changes. An initial hydrostatic fluid pressure field was assumed while the thermal gradient was set to 0.020217˚C/m with an initial temperature of 33.9˚C at the depth of the drift (assumed to be 1478 m depth). Within the drift, the temperature is set to 20.11˚C, a relative humidity of 90% and atmospheric gas pressure (1 bar). Upper and lower boundary conditions were set to constant temperature and pressure conditions, in equilibrium with the initial conditions, and the lateral vertical boundaries were set to no flow conditions. Simulations were executed for 50 years, with the drift wall temperature held a 20.11˚C, and a rock thermal conductivity of 5 W/m K. Simulation results showed good comparison against the kISMET survey (Roggenthen and King, 2017), as shown in Figure 4.

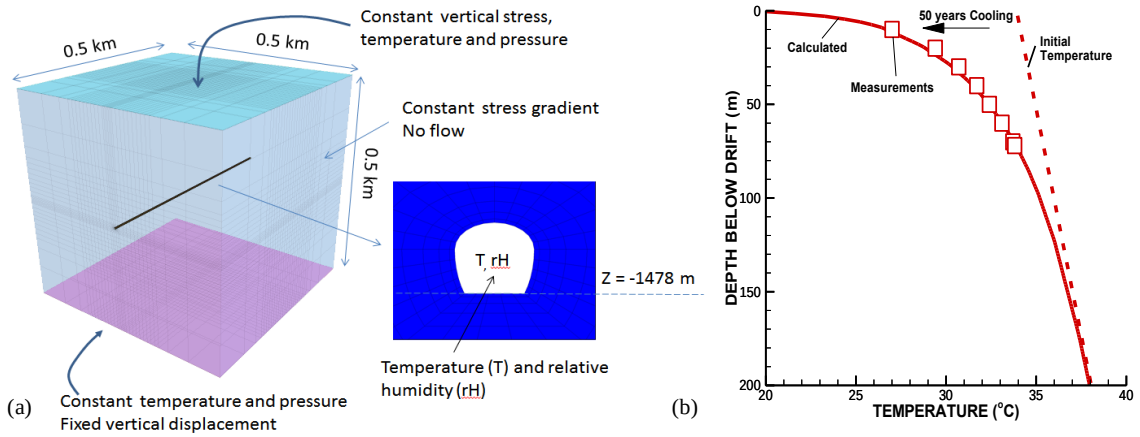

Figure 4: LBNL thermal simulation (a) 3-dimensional model geometry and boundary conditions, (b) results compared against kISMET survey.

3.2 PNNL Modeling and Simulation Team Study

The PNNL team developed a 2-dimensional computational domain with an area of 100 m x 200 m, modeling ½ of the drift domain. A series of numerical simulations were executed, with STOMP-GT (White and Oostrom, 2006), to determine the temperature, pore pressure, and fluid saturation profiles around the 4850 Level West Access Drift at SURF. These profiles were controlled by the ambient geothermal gradient, hydrological state and the historical mining operations. Temperature measurements taken during the underground reconnaissance for the DUSEL facility (Dobson and Salve, 2009) and during the EGS-Collab project within the kISMET boreholes (Oldenburg et al., 2016; Roggenthen and King, 2017) were used for verification of the numerical simulation results. The 4850 Level West Access Drift at SURF was excavated during the mining activities of the Homestake Gold Mine, which began in the late 1870s and continued until 2001, with cessation of mine production. Dewatering of the mine continued for two years, but on June 10, 2003 the pumps were switched off and the mine closed. The Homestake mine workings advanced in depth and lateral spread over time in a complex pattern, driven by the search for higher-grade ore bodies, but the overall depth of the mine increased at a fairly uniform rate of 26 m/yr (Murdoch et al., 2012). Assuming that the water level in the mine followed the progression of the mine workings, drifting of the 4850 Level started in early 1949 (Murdoch et al., 2012). Anderson (1983) modeled temperature profiles around the 8000 Level drift, with a two-dimensional finite-element model. Following cessation of mining operations in 2001 and then active dewatering in 2003, the water level in the mine increased from steadily at a rate of 0.56 m/day (Davis et al., 2009), with the water level reaching the 8000 Level on June 17, 2003. Extrapolating the Davis et al. (2009) data to the 4850 Level, yielded a flooding date of September 1, 2007. Table 4 documents the chronological events associated with modeling the profiles around 4850 Level West Access Drift at SURF.

Table 4. 4850 Level Modeling Events Chronology

Days	Date	Event	Drift-Wall Boundary Conditions
0	3/3/1949	4850 Level Drifting Starts	Advective, 26.0˚C, 5.0 W/m^2 K
19,829	6/17/2003	Homestake Mine Closed	Adiabatic, Zero Flux
21,366	9/1/2007	4850 Level Flooded	Adiabatic, Zero Flux
21,986	5/13/2009	4850 Level Dewatered	Evaporative, 26.0-20.2˚C, 1.5 m/s, 0.85 RH, 5.0 W/m^2 K
22,014	6/10/2009	4850 Level LBNL Survey Start	Evaporative, 26.0-20.2˚C, 1.5 m/s, 0.85 RH, 5.0 W/m^2 K
22,061	7/27/2009	4850 Level LBNL Survey End	Evaporative, 26.0-20.2˚C, 1.5 m/s, 0.85 RH, 5.0 W/m^2 K
24,904	5/9/2017	4850 Level kISMET Survey	

The conceptual model for the numerical simulations was that the phyllite rock surrounding the 4580 Level West Access Drift was homogeneous with constant intrinsic properties and void of hydraulically conductive fractures. Simulations were executed on a structured boundary fitted 2-dimensional domain that extended horizontally 100 m from the drift center line, and 100 m vertically in both directions from the drift mid-height. The outer lateral boundary condition was set to be hydrostatic with a geothermal gradient, with a reference pressure of 14.674 MPa at a depth of 1576.48 m, and a reference temperature of 36.42˚C, at a reference depth of 1572.76 m, with a geothermal gradient of 0.02097 ˚C/m (i.e., increasing with depth). The boundary condition on the drift wall, ceiling, and floor varied with time, as shown in Table 4. During the period from 1949 through the mine closure in 2003, an advective boundary condition was applied with a constant air temperature of 26 ˚C, and an overall heat transfer coefficient of 5.0 W/m^2 K. The advective boundary condition did not consider drying of the rock adjacent to the drift. During the period between mine closure and dewatering of the 4850 Level, an adiabatic, zero flux boundary condition was applied. This boundary condition ignores heat transfer and fluid flow between the phyllite and drift, and does not consider the heat capacitance of air and water in the drift. At the point of dewatering it was assumed that the rock was saturated. An evaporative boundary condition was then applied with a drift air temperature that decreased from 24˚C to 20.2˚C between 2009 and 2017, an air velocity of 1.5 m/s, and an air relative humidity of 85%. An advective heat transfer coefficient of 5.0 W/m^2 K was additionally applied. Simulations were initialized with an aqueous saturation of 1.0, with a pressure of 14.637 MPa at a depth of 1572.76 m and pressure gradient of 0.0098 MPa/m (i.e., increasing with depth), and a temperature of 36.42˚C, at a reference depth of 1572.76 m, with a geothermal gradient of 0.02097 ˚C/m (i.e., increasing with depth). Petrophysical properties of the phyllite used in the numerical simulation are listed in Table 5. Values for grain density, and grain specific heat were equivalent to those used by Ashworth (1983) in the numerical simulations of the 8000 Level drift. Thermal conductivity and intrinsic permeability were determined from 1-dimensional simulations of drift cooling with evaporation, compared against the kISMET measurements of Roggenthen (2017). Ashworth (1983) determined a thermal conductivity of 3.6 W/m K from laboratory measurements, lower than the value of 5.0 W/m K, used in this study. The capillary pressure versus saturation function was the van Genuchten (1980) model with a Webb extension (Webb, 2000), and the aqueous and gas relative permeabilities were computed from the Mualem model.

Two series of temperature measurements served as verification marks for the numerical simulations. Shortly after dewatering of the 4850 Level, Dobson and Salve (2009) made measurements of the temperature of the phyllite rock in a new horizontal borehole drilled to a depth of approximately 2.4 m (i.e., 3.2 m from the drift centerline) and air temperature measurements. The temperature in the borehole showed a decay from 28.58˚C to 26.90˚C over a period of 47 days. These measurements provided a verification of evaporative cooling rates. At the start of the EGS Collab project Roggenthen (2017) made a series of measurements in the near vertical kISMET #3 (Oldenburg et al.,

Table 5. 4850 Level Phyllite Petrophysical Properties

Property	Value	Property	Value	Property	Value
Grain Density	2900 kg/m^3	Intrinsic Permeability	5.0 x 10^{-18} m^2	van Genuchten m	0.346
Porosity	0.01	Thermal Conductivity	5.0 W/m K	Residual Saturation	0.06
Pore Compressibility	7.2 x 10^{-16} 1/Pa	van Genuchten α	0.186 1/m	Oven Dry Head	1.0 x 10^5 m
Grain Specific Heat	805 J/kg K	van Genuchten n	1.529		

2016) borehole. These measurements provided a verification of the current temperature profile around the 4850 Level drift. The temperature and aqueous saturation profiles for 05/09/2017, the time of the kISMET measurements (Roggenthen, 2017), is shown in Figure 5. The temperature profile shows both the impact of the long-term drift cooling which occurred from 1949 through 2003, and then the more recent higher-rate evaporative cooling from 2009 through 2017. The impact of evaporative cooling is time limited, as thin dryout region develops around the drift wall, reducing relative permeability of the rock and evaporation rate.

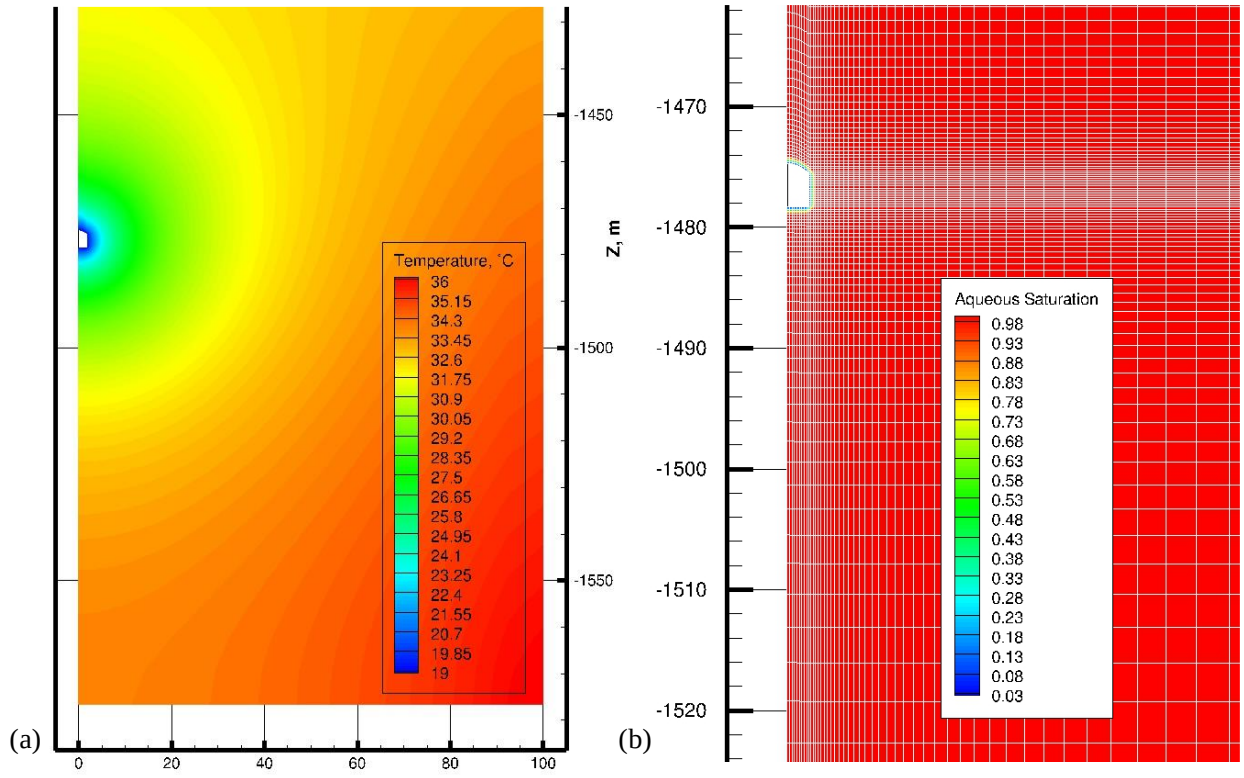

Figure 5: Numerical simulations of (a) temperature profiles around 4850 Level Drift at 05/09/2017, (b) aqueous saturation profiles around 4850 Level Drift at 05/09/2017.

Linear temperature profiles at six points in time along a horizontal line from the drift wall to the outer later boundary, reference from the drift centerline, are shown in Figure 6(a). The initial condition is set at the start of 4850 Level drifting at 03/03/1949. At the time of mine closure on 06/17/2003, the impact of advective cooling can be seen, reducing the temperatures in a radial pattern around the drift. During the mine closure, the adiabatic, zero-flux boundary conditions on the drift wall, yielded recover of the temperature profile, with the drift wall reaching approximately 32˚C. With dewatering of the 4850 Level, evaporative cooling resulted in a rapid decline in the near drift temperature, and the numerical simulations show good agreement with the measurements, both in terms of magnitude and change over the 47-day period, taken during the LBNL survey (Dobson and Salve, 2009). Linear temperature profiles at six points in time along a vertical line from the drift floor to the lower horizontal boundary, reference from the mine surface, are shown in Figure 6(b). Similar trends in the temperature profiles over time are observed in these plots as the system is generally dominated by radial heat transport and fluid flow. The kISMET #3 borehole measurements (Roggenthen, 2017) are shown as makers on the plot. The numerical simulation results at 05/09/2017 show similar profiles, with a slight offset. Whereas, the LBNL survey (Dobson and Salve, 2009) measurements are a strong indicator of evaporation rates, the kISMET survey (Roggenthen, 2017) provides an indication of the total history of the 4850 Level, for which there is little information about conditions within the drift. The objective of this numerical study was to develop temperature profiles around the 4850 Level West Access Drift that could be used as initial conditions for future thermal circulation experiments, but also in support of the fracture stimulation activities, associated with Experiment 1. Temperatures obtained from the two surveys provided

verification marks for defining simulation parameters and setting early-time boundary condition values for the drift. Optimization simulations could be executed to yield improved parameter fits, but would not greatly alter the resulting temperature profiles.

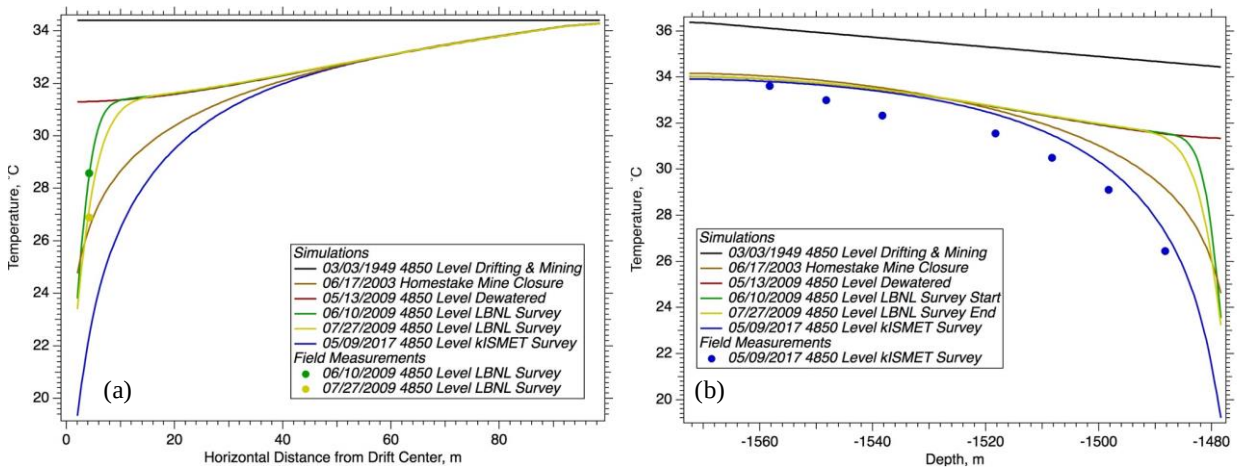

Figure 6: Temperature profiles (a) along a horizontal line from the 4850 Level drift wall (referenced from the drift centerline), (b) along a vertical line from the 4850 Level drift floor (referenced from the mine surface).

4. HYDRAULIC FRACTURING UNDER A STRESS GRADIENT

Prior to selecting the site for the EGS Collab Experiment 1 numerical simulations were executed to forecast fracturing pressures, fracture propagation, fluid circulation rates, and thermal drawdown. In general, these scoping simulations considered vertical gradients in stress and mechanical stress alterations due to the mine workings, but none considered stress alteration due to thermal cooling of the experimental rock volume to cooling and ventilation in the drift. The resulting fractures from these scoping calculations were generally penny shaped. A numerical analysis by the LLNL team additionally considered the impact of stress heterogeneity, by assigning a randomly generated heterogeneity with standard deviation of 0.5, 0.25, and 0.125 MPa on σ_h. These simulations revealed the strong impact of stress heterogeneity on fracture shape, aperture, and circulation flow rates, as shown in Figure 7. With the selection of the site for Experiment 1 at the 4850 Level near the kISMET site (Oldenburg et al., 2016) and the expectation that the experimental rock volume would have experienced cooling, a temperature survey was made in the kISMET boreholes (Roggenthen and King, 2017). These measurements and the subsequent modeling of the temperature profiles around the 4850 Level drift, as described above, indicated the need for the fracture stimulation and fluid circulation modeling to consider potential impacts to the stress field due to rock volume contraction with thermal cooling of the rock from the drift. The modeling and simulation teams from three groups, LLNL, LBNL, and INL addressed this problem.

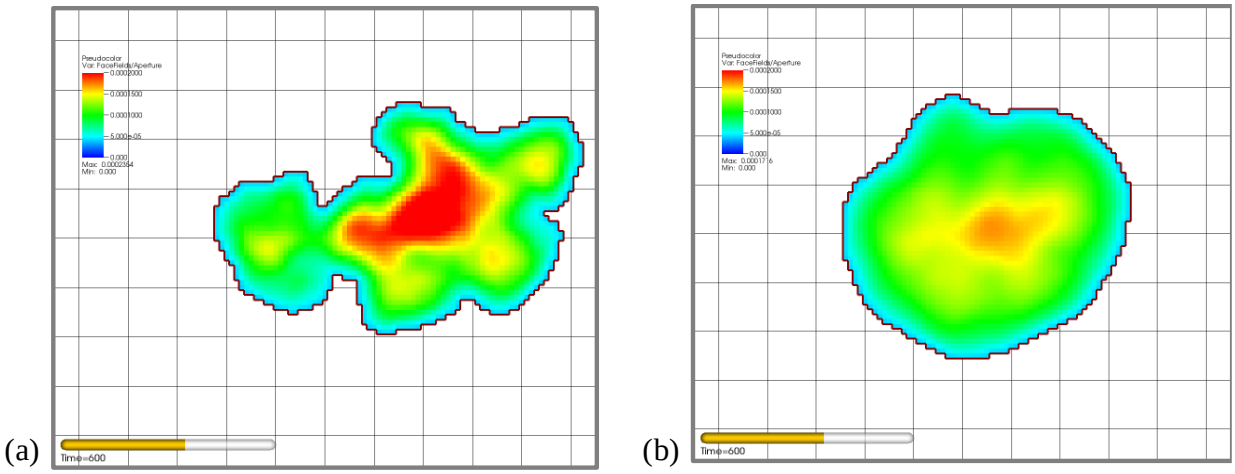

Figure 7: Numerical simulation of fracture propagation with different realizations of σ_h with a mean of 20 MPa, and vertical gradient of 14 kPa/m (a) standard deviation = 0.5 MPa, (b) standard deviation = 0.125 MPa.

4.1 LLNL Modeling and Simulation Team Study

The LLNL team first computed alterations to the stress field caused by the drift, then considered the impact of these stress alterations on hydraulic fracture propagation. To compute the altered stress field, the LLNL team built a solid finite element model, using their GEOS (Settgast et al., 2017), aligned with the drift. The solid finite-element model comprised 4.3 million hexahedral elements, with a mesh resolution of 0.45 m nearest the drift, and a total volume of 200 m x 300 m x 100 m. The stress state was initialized with recent estimates (Oldenburg et al., 2016), with the stress components having a linear vertical gradient, with a zero-value at the ground surface. The finite-

elements within the drift volume were then removed and temperature field around the drift, described above, was imposed and an altered stress state was computed.

A hydraulic fracture tends to propagate perpendicular to the σ_h direction (King and Willis, 1957) and also tends to propagate toward regions with lower stresses. Since the majority of the energy input in a hydraulic stimulation is used to overcome the compressive stress acting on the fracture plane, the most important mechanism through which the drift affects the fracture propagation is its influence on the minimum principal stress. Figure 8 shows the temperature field (a) and the magnitude of minimum principal stress (b) along the expected fracture plane (N94°W, 78° dipping). The results show that the temperature perturbation caused by the drainage and ventilation history of the drift has reached the planned fracturing location and so has the corresponding stress alteration. Assuming fracture initiation for Experiment 1 will occur at a depth of 60 m from the injection borehole collar, the initiation point would be approximately 50 m from the drift axis along the fracture plane. The horizontal gradient of σ_h at this location is approximately 40 kPa/m, which is more than four times the hydrostatic pressure gradient. Consequently, the hydraulic fracture is expected to have a strong tendency to propagate toward the drift. The results also suggest that the presence of the drift reduces the pressure required to propagate a hydraulic fracture at this location by one to two MPa. This reduction would become much more significant if the hydraulic fracture is to be initiated closer to the drift (shallower along the stimulation well), but its tendency to propagate toward the drift and the associated risk of intersecting the drift would also become greater.

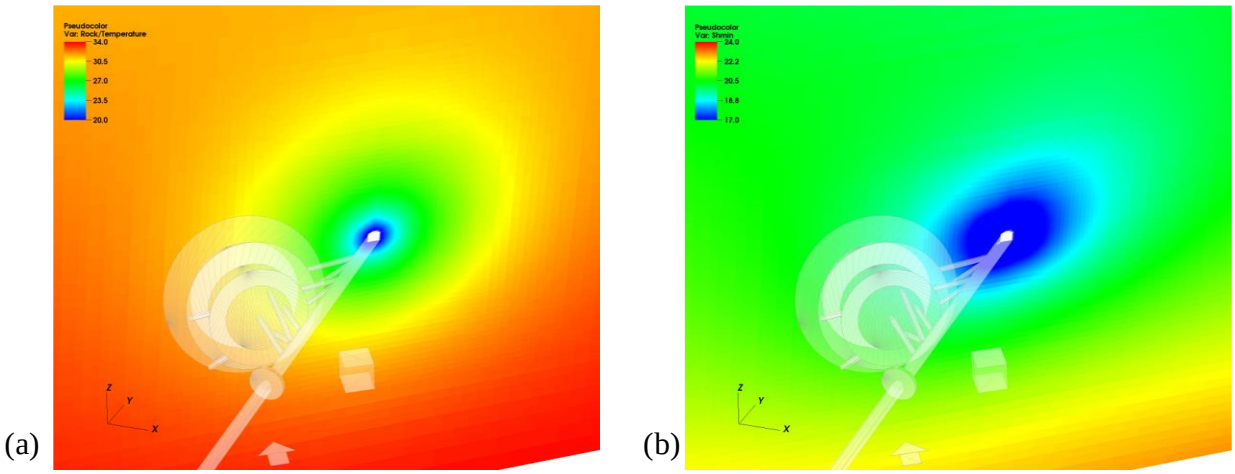

Figure 8: The (a) temperature and (b) stress (minimum principal stress) perturbations caused by the drift along the expected fracture plane. The profiles of the drift, the planned wells, and the hypothetical fractures are shown in semi-transparency.

The LLNL team next modeled hydraulic fracture propagation within the altered stress field described above. For these simulations, the team used their fully coupled hydraulic fracture simulation code GEOS (Fu et al., 2013; Settgast et al., 2017). To simulate hydraulic fracturing, GEOS couples a finite element method (FEM) for mechanical response of the solid matrix, a finite volume method (FVM) based on lubrication theory for the fluid flow along fractures, and the linear elastic fracture mechanics (LEFM) for the fracturing criterion. New fracture area is generated by duplicating the "face element" connecting two adjacent solid elements in the original continuum body. New face flow elements are thereby added to the fracture flow system. The FEM and FVM are naturally coupled: the fluid pressure from the flow module is applied to the surface of the fracture in the solid mesh, while the solid deformation determines the aperture (which in turn determines hydraulic impedance and storage) of the fracture. The mesh for the hydraulic fracturing simulation was different from that for the thermal stress calculation in a number of ways. To make the simulation computationally tractable, the mesh had a lower resolution, 0.9 m near the drift and around the expected hydraulic fracturing trajectory. Prism elements were used to generate grid lines/planes complying with the drift boundaries and the expected fracture plane. Approximately 1.7 million prism elements were used in the simulation. The same mechanical and thermal boundary conditions as those for the thermal stress analysis were applied to the hydraulic fracturing model. The fluid injection point (where the hydraulic fracture was initiated) was 38.4 m to the left of and 14.0 m below the axis of the drift. The distance between the injection point and the drift axis was approximately 51 m along the expected fracture plane. Water with a nominal viscosity of 1.0 cP was injected at a rate of 0.1 L/s, which is in the higher end of the planned stimulation rate. The critical stress intensity factor (K_{IC}, commonly known as the "toughness" of the rock) was assumed to be 1.0 MPa·m$^{0.5}$. The resulting fracture from this simulation was unlike the classical penny shape, showing a strong tendency to migrate toward the drift following the decreasing gradient of σ_h. An interesting feature of the fracture was that aperture decreased migrating away from the injection borehole, but then increased as the fracture approached the drift. Detailed results on hydraulic fracturing under the influence of stress alteration caused by the drift are presented in Fu et al. (2018) and not repeated here.

4.2 LBNL Modeling and Simulation Team Study

The LBNL team conducted thermo-hydro-mechanical (THM) modeling of the Experiment 1 site to quantify the impact of the drift on stress redistribution from the drift excavation itself, as well as that from cooling and mine dewatering. Simulations executed by the LBNL team were completed with the TOUGH-FLAC simulator (Rutqvist, 2011), using a 3D model of the tunnel with the in-situ stress field oblique to the drift according to the best estimate of the stress field from the previous stress measurements conducted for the KISMET project (Oldenburg et al., 2016), as shown in Figure 9(a). The LBNL team considered a number of stress fields and pressure conditions.

The base-case model used the best estimate from the kISMET report (Oldenburg et al., 2016), per Figure 9(b), and two additional cases were considered that varied σ_H, per Figure 9(c) and 9(d). The model setup for these simulations was identical to that for the LBNL team's temperature profile modeling, shown in Figure 4(a), which additionally included coupled pressure evolution modeling. The LBNL simulation results indicate significant changes in the stress field around the drift could occur as a result of cooling and drainage, as shown in Figure 10(a) and 10(b), respectively. The magnitude of this stress change was a function of temperature changes, thermal expansion coefficient and elastic properties. For the LBNL simulations, the coefficient of linear thermal expansion was assumed to be 1 x 10^{-5} $^{\circ}C^{-1}$. Figure 10(b) shows that the combined effect of cooling and drainage gives rise to even more significant stress reduction. The drainage induced stress reduction was caused by poro-elastic stress change which was a function of elastic properties and poro-elastic constants such as the Biot's coefficient. For both cooling and drainage induced stress changes, the calculation shows that the minimum stress could be reduced by as much as 5 MPa at the center of the proposed fracture. The LBNL team compared their simulation results for stresses against stress estimates from the instantaneous shut-in pressure measurements taken in the kISMET boreholes (Oldenburg et al., 2016). This comparison suggested that the combined cooling and drainage stress changes overestimated the stress alterations, and that stress changes due to cooling alone showed better agreement.

The LBNL team then considered the potential impacts of the altered stress field on fracture propagation in Experiment 1. For this portion of their study the team opted to only consider stress alterations due to cooling, ignoring the depressurization induced changes. The team specifically investigated whether the fracture propagation direction would change with depending on the degree of anisotropy in the principal stresses. As the magnitude of σ_H was the least certain, the LBNL team chose to alter this parameter, as indicated in Figures 9(b) through 9(d). Fracture propagation trajectories are shown in Figures 10(a) and 10(c), for $\sigma_H = 2\ \sigma_h$ and $\sigma_H = 1.2\ \sigma_h$, respectively, against the σ_h field considering cooling induced stress changes; where, the trajectory is assumed follow the normal to σ_h. For $\sigma_H = 2\ \sigma_h$, the most anisotropic case considered, shown in Figure 10(a), the fracture trajectory is forecast to be straight to a 20-m radius and beyond. For $\sigma_H = 1.25\ \sigma_h$, the least anisotropic case considered, shown in Figure 10(c), the fracture trajectory is forecast to be straight to a 10-m radius, but could turn toward the drift beyond that. All simulations indicate a gradient of reduced stress toward the drift. Three principal conclusions were drawn by the LBNL team from their simulation study:

1. Cooling and pressure depletion around the drift have the potential of inducing significant changes in the stress field at the proposed fracture experimental location.
2. The main impact of cooling could be a lowering of the fracturing pressure and a gradient of reduced stress that could potentially draw the fracture toward the tunnel.
3. The fracture could turn towards the drift, but this effect would not occur within 10 m radius.

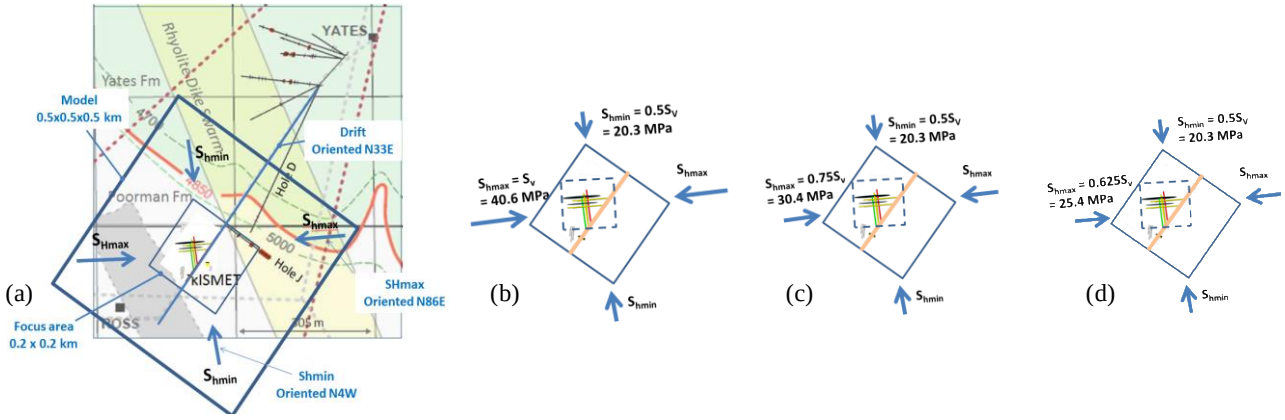

Figure 9: Location of THM model and orientation of principal stresses, (a) orientation within geologic structure on the 4850 Level, (b) base case stress field with $\sigma_H = \sigma_v = 2\ \sigma_h$, (c) case 2 stress field with $\sigma_H = 0.75\ \sigma_v = 1.5\ \sigma_h$, (d) case 3 stress field with $\sigma_H = 0.625\ \sigma_v = 1.25\ \sigma_h$

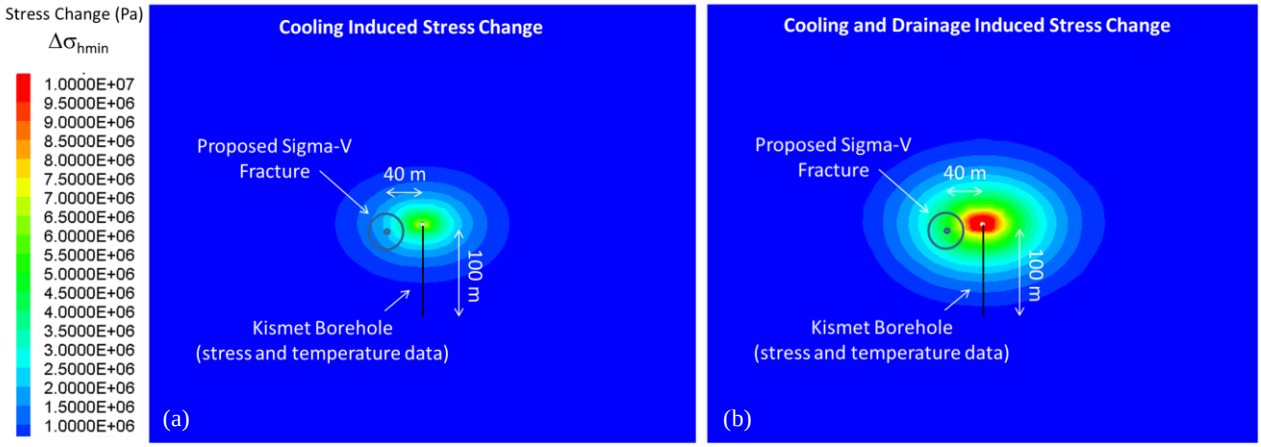

Figure 10: Changes in σ_h due to (a) cooling of the rock, and (b) cooling and drainage of the rock

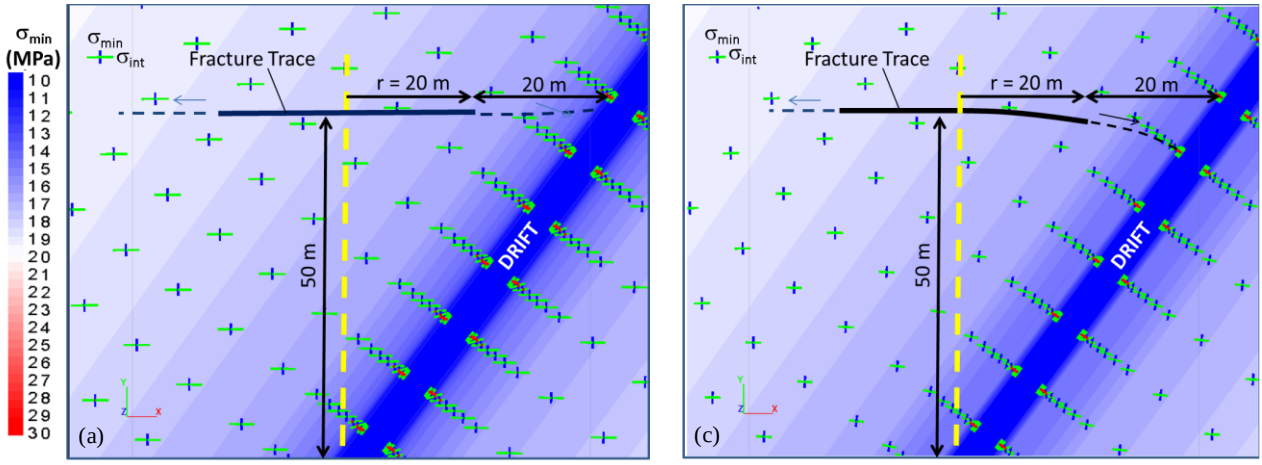

Figure 11: Stress tensor, minimum compressive stress distribution, and expected fracture trace perpendicular to σ_h for 50 years of cooling induced stress effects (a) $\sigma_H = 2\ \sigma_h$ (base case), and (c) $\sigma_H = 1.25\ \sigma_h$ (case 2).

4.3 INL Modeling and Simulation Team Study

The INL team approached the problem of fracture propagation under the effects of cooling induced stress changes via two distinct numerical approaches: 1) the extended finite element method (XFEM) with the commercial Abaqus code, and 2) the discrete element method (DEM) with the INL DEM simulator (Zhou et al., 2017). The temperature profile around the 4850 Level drift for both modeling approaches were derived from an Abaqus thermo-mechanical FEM simulation that considered advective cooling by the drift over a 50-year period, which showed a good comparison against the kISMET borehole survey (Roggenthen and King, 2017). Altered stress fields, considering both mine workings and drift cooling, computed with both the Abaqus XFEM and the DEM simulator, showed agreement between the two numerical methods, with the DEM method having more variability due to the assigned heterogeneities in DEM connections. Fracture propagation simulations were executed with the DEM simulator at two injection rates, 2 and 4 L/s; and with the Abaqus XFEM simulator at 3 L/s. A comparison of the state of the fracture near the time of arrive at the drift is shown in Figure 12 for the different flow rates and numerical approaches. Fracture propagation in Experiment 1 is designed to halt near the production borehole, therefore, these simulations are most informative in understanding the full influence of the stress gradient on fracture propagation, especially as the gradient steepens near the drift. The three simulations shown in Figure 12 show good agreement across the distinct different numerical approaches, in terms of fracture shape characteristics and aperture distributions. In all simulations fractures initial form with a penny shape, but then deform into a more elongated shape, with preferential migration toward the drift over time. The maximum extent of the fracture is greatest with injection rate. Aperture variation across the fracture increases with injection rate, but the aperture distribution character is similar, with the lowest apertures around the fringe of the fracture, higher apertures around the injection borehole, moderate apertures away from the injection borehole, increasing toward the drift in response to gradient of reduced stress toward the drift.

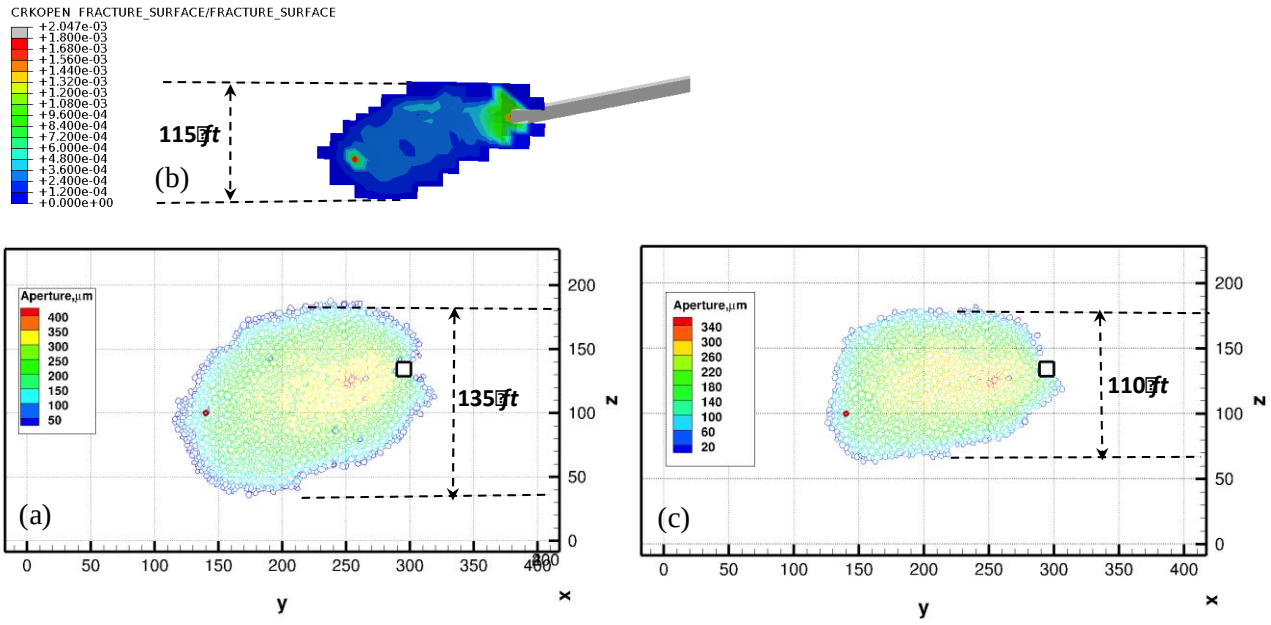

Figure 12: Fracture state in terms of spatial extent and aperture (a) DEM simulation at an injection rate of 4 L/s, (b) Abaqus XFEM simulation at an injection rate of 3 L/s, and (c) DEM simulation at an injection rate of 2 L/s.

5. CONCLUSIONS

The extreme temperature and depth environments of enhanced geothermal systems (EGS) make experimental investigations challenging and costly as proven by the hot-dry rock experiments at Fenton Hill, New Mexico, USA. The United States Department of Energy, Geothermal Technologies Office (GTO) seeks to establish a new field-scale EGS research facility, the Frontier Observatory for Research in Geothermal Energy (FORGE), and currently is in the set-up and characterization stage of selecting a site. In the interim GTO is supporting a collaborative study that will serve as a research and development path between the more conventional laboratory-scale stimulation and rock mechanics experiments and the field-scale studies envisioned for FORGE. This collaborative study, called EGS Collab, is being led by the Lawrence Berkeley National Laboratory (LBNL) and involves other national laboratories, universities and private industry teaming to conduct stimulation and circulation experiments, and verify computer codes, numerical algorithms and approaches, and process models against the generated data. This three-year project has been tasked with providing new knowledge and modeling capabilities, forming a path from laboratory scale to the field scale of FORGE.

Numerical simulation is an essential component of the EGS Collab project in two respects. First numerical simulation is contributing to the design of the meso-scale experiments that will be conducted under *in-situ* stress conditions and crystalline rock formations. Second the experimental measurements will serve as benchmarks against which to compare post-experimental numerical simulations. Heterogeneities in the rock fabric, natural fractures, spatial variations of *in-situ* stress, and other geologic features generally preclude numerical simulation from providing accurate matches to experimental outcomes. The true value of numerical simulation then comes from the understanding it provides concerning complex system behavior, allowing scientists and engineers to make informed choices about experimental designs and interpreting experimental observations. This paper was specifically concerned with addressing ten questions associated with the EGS Collab Experiment 1, and highlights numerical studies in three topical areas: 1) borehole notching, 2) thermal environment surrounding the drift, and 3) hydraulic fracturing under a stress gradient.

The essence of the EGS Collab Experiment 1 is straightforward: 1) create a hydraulic fracture of 10-m radius from an injection borehole, intersecting a production borehole, 2) instrument the experimental volume to resolve the created fracture and characterize mechanical, thermal, and hydrologic state, and 3) circulate chilled fluid between the injection and production boreholes. Developing a sound experimental design, however, required an iterative process of conceptualization and verification via numerical simulation. This process was implement through the evolution of the design, starting with the simple question of borehole orientation, through understanding the impact of fracture propagation on the altered stress state in the experimental volume caused by drift excavation, ventilation, and dewatering. Numerical simulators applied to answer experimental design questions were varied numerical approaches and development teams, but overall yielded equivalent understandings of the fracturing and circulation processes, and generally showed good quantitative agreement. Whether intentional or not many of the numerical simulations studies supporting this experimental design are forecasts, and the outcomes and observations made over execution of Experiment 1 will verify those forecasts and determine the direction of future code developments and applications.

ACKNOWLEDGMENTS:

This material was based upon work supported by the U.S. Department of Energy, Office of Energy Efficiency and Renewable Energy (EERE), Office of Technology Development, Geothermal Technologies Office, under Award Number DE-AC52-07NA27344 with LLNL, Award Number DE-AC05-76RL01830 with PNNL, and Award Number DE-AC02-05CH11231 with LBNL. Publication releases for this manuscript are under LLNL-CONF-744968 and PNNL-SA-131601. The United States Government retains, and the publisher, by

accepting the article for publication, acknowledges that the United States Government retains a non-exclusive, paid-up, irrevocable, world-wide license to publish or reproduce the published form of this manuscript, or allow others to do so, for United States Government purposes. The research supporting this work took place in whole or in part at the Sanford Underground Research Facility in Lead, South Dakota. The assistance of the Sanford Underground Research Facility and its personnel in providing physical access and general logistical and technical support is acknowledged.

REFERENCES

Ashworth, E.: The applications of finite element analysis to thermal conductivity measurements, *Master of Science Thesis*, South Dakota School of Mines and Technology, Rapid City, South Dakota (1983).

Blacker, T., Owen, S.J., Staten, M.L., Quadros, R.W., Hanks, B., Clark, B., Hensley, T., Meyers, R.J., Ernst, C., Merkley, K., Morris, R., McBride, C., Stimpson, C., Plooster, M., Showman, S.: *CUBIT Geometry and Mesh Generation Toolkit 15.3 User Documentation*, SAND2017-6895W, Sandia National Laboratories, Albuquerque, NM, USA (2017).

Brown, D.W., Duchane, D.V., Heiken, G., and Hriscu, V.T.: *Mining the Earth's Heat: Hot Dry Rock Geothermal Energy*, Springer, New York. https://doi.org/10.1007/978-3-540-68910-2 (2012).

Davis, A.D., Stetler, L.D., Roggenthen, W.M., Hladysz, Z.J., and Salve, R.: Instrumentation of the Homestake Underground Laboratory for Drawdown Measurements during Dewatering, *Proceedings*, SME Annual Meeting, Feb. 22-25, 2009, Denver, CO (2009).

Dobson, P.F., and Salve, R.: *Underground Reconnaissance and Environmental Monitoring Related to Geologic CO_2 Sequestration Studies at the DUSEL Facility, Homestake Mine, South Dakota*, LBNL-2858E, Lawrence Berkeley National Laboratory, Berkeley, CA (2009).

Duchane, D.V., and Winchester, W.W.: *Hot Dry Rock Energy Annual Report Fiscal Year 1992*, Los Alamos National Laboratory, LA-UR-93-1678, Los Alamos, New Mexico, USA (1992).

Fu, P., Johnson, S.M., and Carrigan, C.R.: An Explicitly Coupled Hydro-Geomechanical Model for Simulating Hydraulic Fracturing in Arbitrary Discrete Fracture Networks, *International Journal for Numerical and Analytical Methods in Geomechanics*, 37(14): 2278–2300 (2013).

Fu, P., White, M.D., Morris, J.P., and Kneafsey, T.J.: Predicting Hydraulic Fracture Trajectory Under the Influence of a Mine Drift in EGS Collab Experiment I, *Proceedings* of the 43rd Workshop on Geothermal Reservoir Engineering, Stanford University, Stanford, California, February 12-14, (2018).

Gaston, D., Guo, L., Hansen, G., Huang, H., Johnson, R., Park, H., Podgorney, R., Tonks, M., and Williamson, R.: Parallel Algorithms and Software for Nuclear, Energy, and Environmental Applications Part I: Multiphysics Algorithms, *Communications in Computational Physics (Print)*, 12(3):807-833 (2012).

Gaston, D., Guo, L., Hansen, G., Huang, H., Johnson, R., Park, H., Podgorney, R., Tonks, M., and Williamson, R.: Parallel Algorithms and Software for Nuclear, Energy, and Environmental Applications Part II: Multiphysics Software, *Communications in Computational Physics (Print)*, 12(3):834-865 (2012).

Guo, B., Fu, P., Hao, Y., Peters, C.A., and Carrigan, C.R.: Thermal drawdown-induced flow channeling in a single fracture in EGS, *Geothermics*, 61, (2016), 46–62.

Mualem, Y.: New Model for Predicting Hydraulic Conductivity of Unsaturated Porous-Media, *Water Resources Research*, 12(3):513-522, doi:DOI 10.1029/WR012i003p00513 (1976).

Murdoch, L.C., Germanovich, L.N., Wang, H., Onstott, T.C., Elsworth, D., Stetler, L., and Boutt, D..: Hydrogeology of the vicinity of Homestake mine, South Dakota, USA, *Hydrogeology Journal*, 20:27-43, doi 10.1007/s10040-011-0773-7 (2012).

Oldenburg, C.M., Dobson, P.F., Wu, Y., Cook, P.J., Kneafsey, T.J., Nakagawa, S., Ulrich, C., Siler, D.L., Guglielmi, Y., Ajo-Franklin, J., Rutqvist, J., Daley, T.M., Birkholzer, J.T., Wang, H., Lord, N.E., Haimson, B.C., Sone, H., Vigilante, P., Roggenthen, W.M., Doe, T.W., Lee, M.Y., Ingraham, M., Huang, H., Mattson, E.D., Zhou, J., Johnson, T.J., Zoback, M.D., Morris, J.P., White J.A., Johnson, P.A., Coblentz, D.D., and Heise, J..: *Intermediate-Scale Hydraulic Fracturing in a Deep Mine, kISMET Project Summary 2016*, LBNL-1006444, Lawrence Berkeley National Laboratory, Berkeley, CA (2016).

Podgorney, R.K., Huang, H., and Gaston, D..: A Fully-Coupled, Implicit, Finite Element Model for Simultaneously Solving Multiphase Fluid Flow, Heat Transport, and Rock Deformation. *Proceedings*, Geothermal Resources Council Annual Meeting, Sacramento, CA (2010).

Roggenthen, W.M., and King, D.K.: Quick Review of T data for kISMET Area (5/19/17), *Unpublished EGS Collab Project Report*, Lawrence Berkeley National Laboratory, Berkeley, CA (2017).

Rutqvist, J.: Status of the TOUGH-FLAC simulator and recent applications related to coupled fluid flow and crustal deformations. *Comput. Geosci.*, 37:739–750 (2011).

Settgast, R.R., Fu, P., Walsh, S.D.C., White, J.A., Annavarapu, C., and Ryerson F.J.: A fully coupled method for massively parallel simulation of hydraulically driven fractures in 3-dimensions, *Int. J. Numer. Anal. Methods Geomech.*, 41(5):627–653 (2017).

U.S. Department of Energy, Energy Efficiency & Renewable Energy, Geothermal Technologies Office. 2016 Annual Report Geothermal Technologies Office, *Retrieved*, https://energy.gov/sites/prod/files/2017/03/f34/GTO%202016%20Annual%20Report_0.pdf. (2017).

Van Genuchten, MTA.: A closed-form equation for predicting the hydraulic conductivity of unsaturated soils, *Soil Science Society of America Journal*, 44:892-898 (1980).

Webb, S.W.: A simple extension of two-phase characteristic curves to include the dry region, *Water Resources Research*, 36(6):1425-1430, doi 10.1029/2000wr900057 (2000).

White, MD and M Oostrom.: *STOMP Subsurface Transport Over Multiple Phases, Version 4.0, User's Guide,* PNNL-15782 (2006).

White, M.D., Fu, P., and McClure, M.W.: Outcomes from a collaborative approach to a code comparison study for enhanced geothermal systems. *Proceedings*, 42nd Workshop on Geothermal Reservoir Engineering, Stanford University, Stanford, CA, USA (2017a).

White, M.D., Fu, P., Huang, H., Ghassemi, A., EGS Collab Team: The role of numerical simulation in the design of stimulation and circulation experiments for the EGS Collab Project, *Proceedings*, GRC Transactions, Vol. 41 (2017b).

White, M.D., McClure, M.W., Fu, P., Cheng, Q., Elsworth, D., Gan, Q., Hao, Y., Im, K.J., Safari, R., Tao, Q., Xia, Y., Podgorney, R.K., Danko, G., Bahrami, D., Chiu, K., Fang, Y., Gao, Q., Horne, R.N., Norbeck, J., Sesetty, V., White, S.K., Kelkar, S., Ghassemi, A., Barbier, C., Detournay, C., Furtney, J.K., Guo, B., Huang, K., Rutqvist, J., Sonnenthal, E., Wong, Z.: *Benchmark Problems of the Geothermal Technologies Office Code Comparison Study*, Pacific Northwest National Laboratory, PNNL-26016 (2016).

Xia, Y., M. Plummer, E. Mattson, R. Podgorney, and A. Ghassemi.: Design, modeling and evaluation of a doublet heat extraction model in enhanced geothermal systems. *Renewable Energy*, 105:232-247, (2017).

Zhou, J., Huang, H., Mattson, E., Wang, H.F., Haimson, B.C., Doe, T.W., Oldenburg, C., and Dobson, P.F.: Modeling of hydraulic fracture propagation at the kISMET site using a fully coupled 3D network-flow and quasi-static discrete element model. *Proceedings*, 42nd Workshop on Geothermal Reservoir Engineering, Stanford University, Stanford, CA, USA (2017).

Zyvoloski, A.G.: *FEHM: A control volume finite element code for simulating subsurface multi-phase multi-fluid heat and mass transfer*. Los Alamos Unclassified Report, LA-UR-07-3359 (2007).